LAWRENCE
LIVERMORE
NATIONAL
LABORATORY

UCRL-TR-203563

Resolving Nuclear Reactor Lifetime Extension Questions: A Combined Multiscale Modeling and Positron Characterization approach

B.D. Wirth, P. Asoka-Kumar, A. Denison, S.C. Glade, R.H. Howell, J. Marian, G.R. Odette, P.A. Sterne

April 16, 2004

Disclaimer

This document was prepared as an account of work sponsored by an agency of the United States Government. Neither the United States Government nor the University of California nor any of their employees, makes any warranty, express or implied, or assumes any legal liability or responsibility for the accuracy, completeness, or usefulness of any information, apparatus, product, or process disclosed, or represents that its use would not infringe privately owned rights. Reference herein to any specific commercial product, process, or service by trade name, trademark, manufacturer, or otherwise, does not necessarily constitute or imply its endorsement, recommendation, or favoring by the United States Government or the University of California. The views and opinions of authors expressed herein do not necessarily state or reflect those of the United States Government or the University of California, and shall not be used for advertising or product endorsement purposes.

This work was performed under the auspices of the U.S. Department of Energy by University of California, Lawrence Livermore National Laboratory under Contract W-7405-Eng-48.

RESEARCH OBJECTIVE

The objective of this work is to determine the chemical composition of nanometer precipitates responsible for irradiation hardening and embrittlement of reactor pressure vessel steels, which threaten to limit the operating lifetime of nuclear power plants worldwide. The scientific approach incorporates computational multiscale modeling of radiation damage and microstructural evolution in Fe-Cu-Ni-Mn alloys, and experimental characterization by positron annihilation spectroscopy and small angle neutron scattering. The modeling and experimental results are

BACKGROUND AND MOTIVATION

Currently nuclear power accounts for approximately 20% of the U.S. supply of electricity. However, over the next two decades, as demand continues to rise, a large number of the ~110 U.S. reactors will reach the end of their operating lifetime. Lifetime extension can provide significant benefit to the electrical supply without contributing to air pollution or greenhouse gas emissions. Yet, the safe and reliable extension of nuclear power plant operating lifetimes depends on maintaining the integrity of structural materials, whose properties degrade as a result of neutron and gamma ray exposure.

From a safety perspective, the most critical structural component in a nuclear reactor is the reactor pressure vessel (RPV), which embrittles during operation due to the leakage of high energy neutrons from the reactor core. Many years of research have established that steel hardening and embrittlement of the reactor pressure vessel results from the formation of a high number density of ultra-fine, nanometer sized copper-manganese-nickel precipitates and sub-nanometer defect cluster-solute complexes. In steels containing > 0.1% copper, the precipitates are the dominant embrittling feature. The sub-nanometer cluster complexes and nanometer-sized precipitates impede dislocation motion, producing a substantial increase in yield stress (hardening) and a corresponding elevation in the cleavage transition temperature (embrittlement) [1].

Yet, two outstanding questions impact predictions of hardening and embrittlement at the increased irradiation exposures that will be experienced during plant lifetime extension. Significant controversy exists regarding i) the chemical composition of the nanometer-scale precipitates [2,3] and ii) the identity of the defect cluster-solute complexes [2].

The nanometer-precipitates in irradiated reactor pressure vessel steels are commonly characterized by three dimensional atom probe (3DAP) tomography and small angle neutron scattering (SANS). These measurements generally reveal similar precipitate-type feature number densities, sizes and Mn and Ni contents, but provide very different views of the nano-precipitate composition. The 3DAP results have been interpreted to suggest that the precipitates are Cu enriched, but contain significant quantities of Fe (> 50%) [3]. In contrast, standard interpretation of a large body of SANS data, including on alloys with systematic variations in the key alloying elements, indicate the presence of well-formed precipitates that contain Cu (typically ~70%), Ni and Mn, but little or no Fe [2]. The practical implications of this viewpoint are enormous, casting doubt upon the physically based models [4] of irradiation embrittlement in RPV steels used by regulators to assess lifetime limits.

The defect cluster-solute complexes had not been identified by experimental characterization techniques prior to this work, although they were known to exist based on

mechanical property degradation (embrittlement) of RPV steels containing little or no copper. Embrittlement models [4] assume an increasing contribution to the overall embrittlement from these defects at higher doses (to be experienced during lifetime extension), yet quantitative understanding of their evolution kinetics and their contribution to embrittlement did not exist.

This LDRD project addressed these two outstanding issues through a combination of physically based multiscale modeling and a novel experimental characterization program to validate the modeling predictions. Specifically, molecular dynamics and kinetic Monte Carlo defect evolution models developed under this LDRD program were able to predict the character of the sub-nanometer vacancy – solute cluster complexes and the composition of the copper precipitates. These predictions were quantitatively validated by positron annihilation spectroscopy measurements, where the key to validation was the direct comparison of predicted positron observables with the actual experiments, through the use of first-principles positron theory.

RESEARCH ACTIVITIES

Irradiation embrittlement results from a multitude of physical processes, spanning a wide range of length and time scales. The inherently multiscale nature of the radiation damage problem requires a hierarchical research approach, which closely combines a multiscale modeling methodology to predict the underlying structural and chemical evolution at the nanoscale, with experiments designed to characterize such features.

Multiscale Modeling

The multiscale modeling methodology involves using *ab initio* electronic structure calculations to validate semi-empirical interatomic potentials and a combination of molecular dynamics (MD) and kinetic Monte Carlo (KMC) simulations over the relevant length and time scales controlling production of primary defects in high-energy displacement cascades and the subsequent long-time evolution to generate late-time vacancy cluster production. This involves combining an MD database of primary damage production with two separate KMC simulations that independently follow the SIA/SIA cluster and the subsequent vacancy evolution. Separation of the time scales between vacancy and SIA/SIA cluster diffusion, naturally leads to the nearly independent evolution of these two populations.

In this approach, we follow the relatively short time (~100 nanosecond at 563 K) evolution of the cascade using ‘defect’-oriented KMC [5]. This allows for additional SIA/vacancy recombination and the migration of SIA and SIA clusters away from the cascade volume and assumed annihilation at system sinks. During this ‘defect’ KMC, the time duration is insufficient for significant vacancy migration and the SIA/SIA clusters are the only diffusing species. Further, we assume that the SIA clusters of size, $N > 5$, migrate in one-dimension.

The ‘defect’ KMC simulations result in an initial configuration for longer time kinetic lattice Monte Carlo (KLMC) cascade aging simulations, which follow the vacancy population evolution. The KLMC simulations are performed in pure Fe and dilute Fe-Cu alloys on a bcc-iron lattice and use embedded atom-method type potentials to describe the unrelaxed lattice energetics. The iron and copper potentials were from Finnis and Sinclair [6] and Ackland et. al. [7], respectively; and the iron-copper potential was developed by fitting the dilute heat of

solution for copper in iron, the copper-vacancy binding energy and the iron-copper {110} interface energy [8].

Within the KLMC model, the specific jump of each vacancy in the system are based on a standard random number Metropolis test, using a modified residence time algorithm to advance the time. In this approach, at least one, and in some cases many more than one, vacancy jump occurs in each KLMC sweep. The initial vacancy fate is to either cluster, with other vacancies or copper atoms, or diffuse to the cell boundary, which is assumed to be a defect sink. Clusters can grow by absorbing single vacancies, which may be emitted from other clusters, or by coalescence with mobile clusters. Emitted vacancies may also annihilate at the cell boundary. The jump rate and sequence depends on the local environment; thus the time increment changes as the cascade evolves. The increments start out short, for unbound, isolated vacancies, but increase enormously as larger bound cluster-complexes develop. As the cluster-complexes grow, the cluster mobility drops and non-emission jumps that change the shape, but not the cluster-complex position or size, become far more probable; hence, the efficiency of the KLMC algorithm decreases dramatically. To circumvent this problem, a 'pulse annealing' technique is used to accelerate the computation of vacancy emission from the clusters.

After six hundred 'inefficient' sweeps, the temperature is increased to identify the weakest bound vacancy to a cluster and determine its most probable emission trajectory. This vacancy is then 'required' to make three additional jumps along its pre-determined trajectory at the actual simulation temperature. Other vacancies in the simulation are also allowed to jump (or not) during this period. The effective time increment adjustment factor for 'pulse annealing' is the ratio of the total jump probability to the product of the probabilities for the pre-selected series of jumps. Emitted vacancies can be captured by the emitting or another cluster or be annihilated at the cell boundary.

Positron Annihilation Spectroscopy

The positron annihilation spectroscopy (PAS) experiments involve measuring positron lifetimes, the Doppler broadening of annihilation photons, and the magnetic polarization of positron annihilation. The PAS technique is unique in its ability to detect the presence of vacancy and vacancy cluster trapping centers and spatial regions of higher local positron affinity, e.g. in precipitates. The key to interpreting PAS experiments is the direct simulation of the experimental observables.

PAS is a well-established technique for detecting open volume regions of a material [9], as well as the chemical identity of the elements surrounding these open volume regions [10]. The positron is the antiparticle of an electron, with the same mass (511 keV/c^2), but a positive charge. Following positron injection into a metal, the positron quickly dissipates its kinetic energy in scattering events and reaches thermal equilibrium (within ~ 3 picoseconds). Due to its positive charge, the positron experiences a repulsive force from ionic cores and an attractive force from electrons, open volume defects, and regions of increased positron affinity. Ultimately, the positron annihilates with an electron, predominantly producing two 511 keV gamma rays traveling in opposite directions.

Each element has a unique positron affinity and the positron will preferentially localize in regions of high positron affinity. The positron affinities of elements important to this work are: Fe, -3.84 eV; Cu, -4.81 eV; Ni, -and Mn, -3.72 eV [11]. As shown by Nagai *et al.* [12], clusters of copper as small as 5-10 atoms in an iron matrix will localize the positron and effectively act as a positron trap. Three different PAS techniques were used in this work. In positron annihilation

lifetime spectroscopy (PALS) the interval between implantation of the positron into a material and its annihilation, as detected by the two 511 keV gamma rays, is measured. By decomposing the lifetime spectrum into one to three distinct lifetime components, the positron lifetime in a material is obtained, with the positron lifetime being characteristic of the positron end-state, or trapping site. Multiple lifetimes are present if one or more trapping defects exist. The positron lifetime strongly correlates with vacancy-cluster (open-volume region) size up to a saturation value characteristic of a planar free surface, as described in more detail by Hautojärvi and Corbel [9].

The two annihilation gamma rays are not actually at 511 keV, due to the conservation of momentum of the electron-positron pair in the direction of the gamma ray emission; these gamma rays are Doppler shifted, one blue and the other red shifted, by an amount of energy

$$\Delta E = \frac{1}{2} p_L c \qquad (1),$$

where p_L is the longitudinal component of the electron-positron momentum in the direction of the gamma ray emission and c is the speed of light. Measurement of both annihilation gamma rays in coincidence allows for precise determination of the Doppler shift, and thus a measurement of the Orbital Electron Momentum Spectra (OEMS) [10]. Each element has a characteristic orbital electron momentum spectrum, resulting from the combination of core and valence electron momentum. Core electrons are more tightly bound to atoms and have a higher electron momentum than valence electrons, making the high momentum region of the OEMS most useful for elemental specificity. By comparing the measured OEMS to theoretically calculated orbital electron momentum spectra [13] or the measured spectra of pure elements, a determination of the chemical identity is obtained in the vicinity of the annihilating positron.

The third PAS technique used was developed specifically within this LDRD program to probe the magnetic character and chemical composition of the nanometer Cu-Mn precipitates and represents the first application of spin-polarized, magnetic positron annihilation measurements of the OEMS of embedded nanometer particles. The underlying principle of using polarized positrons to selectively measure the momentum distribution of minority and majority electrons through magnetic field polarity reversal is well known [14,15]. By using an externally applied magnetic field, the magnetic moment in Fe can be aligned either parallel or anti-parallel to the positron polarity, resulting in preferential annihilation with minority and majority spin electrons respectively, and a corresponding change in the annihilation characteristic with field reversal.

The magnetic moment is defined by the net difference between the majority and minority electrons, i.e. electrons whose spins are aligned parallel or anti-parallel, respectively, to an applied magnetic field. The spin polarized positron annihilation measurements were conducted using positrons from a conventional ^{22}Na radioactive source, which provides a mean depth of ~ 30 microns into the samples. Due to parity non-conservation in beta decay, positrons emitted from the source have their spins aligned parallel to momentum and are guided to the sample with a magnetic field of ~ 1 kG. Coincidence OEMS records two photons from each annihilation event and annihilation into two photons occurs only when the particles have opposite spin. Since the positron polarity is fixed, reversing the direction of the applied magnetic field changes the positron annihilation fraction with majority and minority electrons, resulting in a sensitive and selective probe of the local magnetic moment. Both the radioactive source and the specimen are located in the same external magnetic field. Since depolarization effects are small when non-relativistic positrons are slowed down to thermal energies, it is possible to investigate the

interaction of polarized positrons with changing populations of majority and minority electrons. This technique has been used to probe the momentum distribution of the electrons responsible for ferromagnetism in Fe [16].

Two experimental facilities exist at Lawrence Livermore National Laboratory for PAS measurements of positron lifetime, OEMS and magnetic polarization OEMS. A high-energy mono-energetic positron beam is formed using positrons emitted from a ^{22}Na source placed at the terminal of a 3 MeV electrostatic accelerator [17]. The positron beam (with a typical intensity of 5×10^5 positrons/s) emerging from the accelerator column is focused by a thin solenoid and exits the vacuum through a 25 μm thick Al window. The positrons enter a specimen either directly or after passing through a 2 mm thick scintillator, which provides a start signal for positron lifetime measurements. The positron penetration depth is ~2-3 mm, and allows bulk property measurements without significant contributions from near-surface regions. The annihilation gamma rays are detected using detectors positioned co-linear (for lifetime) or perpendicular (for lifetime and OEMS) with respect to the positron beam. The use of a high energy positron beam allows for bulk specimen characterization, which does not need to be in vacuum, and improves the signal to noise ratio by eliminating background radiation from the radioactive positron source.

The second experimental facility is one in which positrons emitted from a ^{22}Na radioactive source are confined and transported to the sample using a strong magnetic field (~1.0 kG). The positrons have a kinetic energy of ~300 keV, giving a maximum penetration depth in materials of ~30 μm. This setup is used for OEMS measurements on bulk specimens, as well as performing magnetic measurements by using the natural spin polarization of radioactively emitted positrons (spin-polarized, magnetic positron annihilation measurements) [18].

Small Angle Neutron Scattering

SANS measurements were performed as a complement to the PAS investigations, the measurements were performed at the 8-meter beamline at the Cold Neutron Research Facility of the National Institute of Standards and Technology [19]. Samples are measured in a strong magnetic field (≥ 1.8 T $\pm$ 0.1 T) oriented horizontally to saturate the α-Fe matrix. This allows for the measurement of both nuclear (N) and magnetic (M) neutron scattering due to scattering length density differences between the α-Fe matrix and the scattering feature. The neutron scattering at small angles ($\theta \leq 8°$) was measured from a well collimated beam of cold neutrons (λ=0.5 nm) with a two-dimensional 64x64 cm position sensitive detector positioned ~2 m from the sample.

Assuming that the features formed under irradiation, namely the nanometer precipitates and sub-nanometer matrix features, are spherical and non-magnetic in a saturated ferromagnetic iron matrix; log-normal size distributions of one or two spherical scattering features are fit to the absolute scattering cross section data to provide the mean size, number density (N_d), and volume fraction (f_v) of the scattering feature(s). Furthermore, estimates of the scattering feature composition can be made from the measured magnetic to nuclear scattering ratio (M/N). More details regarding the SANS experiments and data analysis can be found in [20-22].

Modeling Experimental Observables

Quantum mechanical calculations of positron states in materials provide accurate, quantitative predictions of both positron lifetime and core-electron momentum distributions. We have recently developed a finite-element approach for solving the Schrodinger equation and

calculating positron observables [13]. This capability represents the key to experimentally validating our multiscale modeling methodology. By coupling the atomic configurations of nanostructural features predicted by multiscale modeling to the finite-element simulations of the experimental observables, we can reach self-consistency and provide the understanding needed to resolve the current controversies about the character and composition of nanostructural features.

RESULTS AND TECHNICAL OUTCOME

Modeling predictions of precipitate and matrix feature structure and composition

A database of approximately five displacement cascades at each PRA energy of twenty, forty and fifty keV served as input to the 'defect' KMC. The primary damage distributions were obtained from from MD simulations provided by R.E. Stoller and are described in more detail elsewhere [23,24]. Approximately 10 'defect' KMC simulations followed the initial (~100 nanosecond) evolution of each independent cascade to provide a statistically significant database of cascade vacancy-rich core distributions. Notably, a large amount of intracascade recombination occurred during this first ~100 ns of aging, as described in Table 1, with more recombination within the higher energy cascades. This likely results from the spatial correlation of sub-cascade lobes which form at higher PRA energies, as well as an increased population of isolated Frenkel pairs between the lobes. The spatial distribution of vacancies remaining after the diffusion, recombination and ultimate annihilation of the SIA/SIA clusters from each simulation serves as an input database for the KLMC simulations.

Table 1 – Surviving number of point defects at the end of the displacement cascade (~100 ps) and after the initial (~100 ns) evolution and diffusion of the SIA/SIA clusters.

Cascade energy (keV)	MD defects (~100 ps)	Surviving vacancies (~100 ns)
20	54	47 (87%)
40	80	72 (72%)
50	176	111 (63%)

Starting from a core rich in (mostly) isolated vacancies, the KLMC simulations in both pure Fe and the Fe-Cu alloys reveal the very rapid formation of a population of small, three-dimensional vacancy clusters and vacancy-Cu cluster complexes, on average requiring only a few vacancy jumps. Subsequently, the clusters migrated, coarsened and dissolved, as shown in Figure 1. Reduction of the net residual vacancy concentration in the cascade core by emission-migration-annihilation events was continuous, but progressively slowed with cluster growth. Clusters grew initially primarily by the coalescence of smaller mobile clusters, and later by emission-absorption processes. A wide range of final dissolution times was observed over multiple simulations of each initial cascade configuration. The mean cluster lifetime of $4x10^5$ seconds in pure Fe, obtained through a large number of simulations from a library of 20, 40 and 50 keV cascades, is in remarkably good agreement with an experimental estimate for the lifetime of unstable matrix defects of $3x10^5$ seconds [25]. Vacancy cluster stabilization occurred as a consequence of the strong binding between oversized Cu solute atoms with individual and clustered vacancies and the mean cluster lifetime increased substantially to $1.5x10^6$ seconds in the Fe-0.3%Cu alloy.

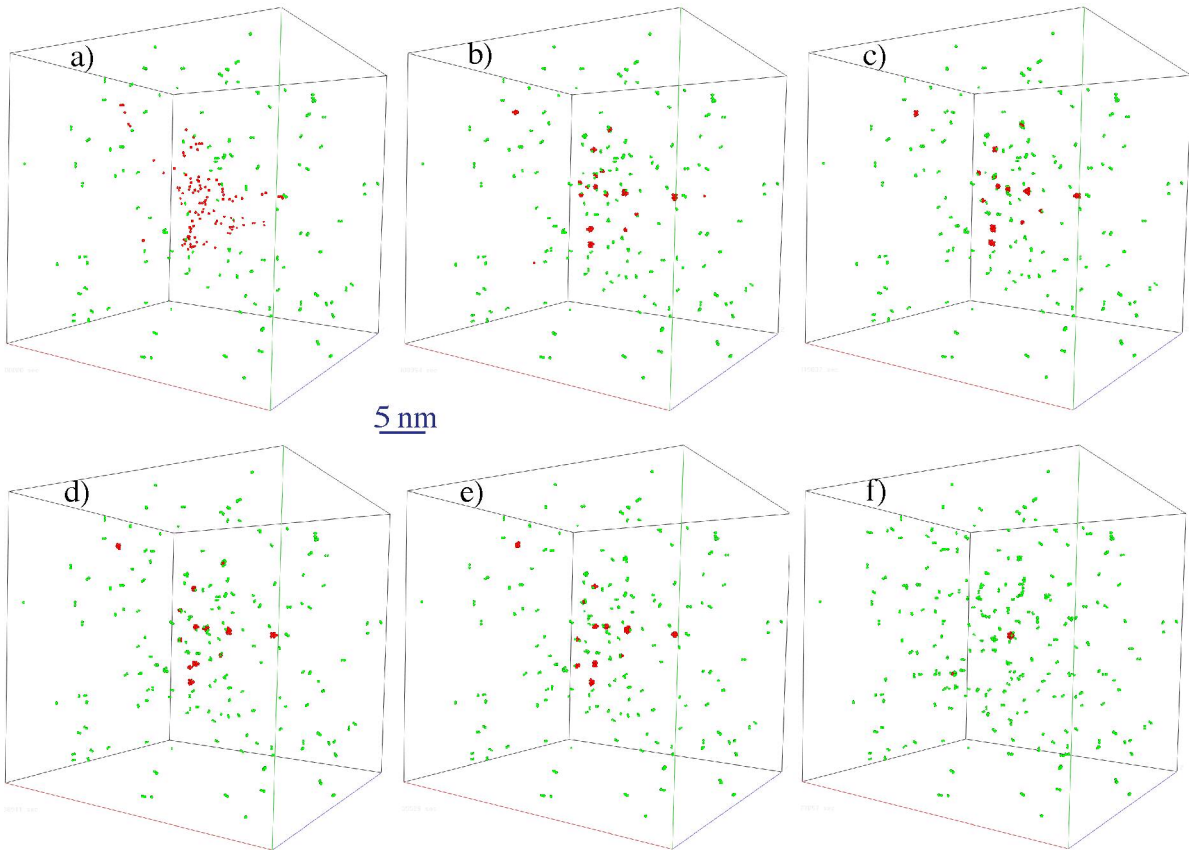

Figure 1. Kinetic Monte Carlo simulation results of the vacancy-Cu evolution a) 200 ps, b) 9 ms, c) 20 ms, d) 5 s, e) 135 s, and f) 1.35×10^6 s following the production of a 50 keV displacement cascade in an Fe-0.3% Cu alloy. Red (dark) circles show the position of vacancies, green (light) circles the clustered Cu atoms.

KLMC simulations of the Fe-0.3%Cu alloy clearly reveal the existence of a continuous distribution of cascade vacancy-Cu (solute) clusters, which constitute both unstable and stable matrix defect features. Small complexes, consisting of less than a total of ten vacancies and copper atoms, were quite mobile and cluster-complex growth occurred by coalescence. Cluster-complexes ranged in size from two to three vacancies with six or more copper atoms to twenty or more vacancies with two to three copper atoms. In general, smaller vacancy clusters were associated with larger numbers of copper atoms. This is partly a result of the high mobility of smaller vacancy complexes, resulting in more local gettering of copper atoms. The larger vacancy cluster-complexes were typically associated with fewer copper atoms, indicative of their relatively low mobility. By the time of complete vacancy dissolution, residual copper clusters ranged in size from 4 to 15 atoms and serve as embryos for copper precipitate formation. Finally, these cascade aging simulations provide the vacancy cluster populations that exist at late times, in addition to the temporal sequence-of-events responsible for the formation of vacancy-Cu cluster complexes, and thus enable the generation of production cross-sections.

Lattice Monte Carlo simulations have also been used to simulate the atomic structure and composition of Cu-Mn-Ni precipitates in body-centered cubic Fe alloys. The results clearly indicate that the precipitates contain a copper rich core, with a relatively diffuse interface that is often enriched in other solutes including Mn and Ni. Notably, these simulations, in addition to

thermodynamic predictions of the precipitate composition do not indicate that substantial (e.g. > 40-50%) Fe is present in the precipitates.

Thus, the key conclusions from the multiscale modeling aspect of the LDRD research program are that the matrix features consist of a population of sub-nanometer vacancy – Cu (and other solute) cluster complexes and that the nanometer-sized precipitates do not contain sizeable fractions of Fe. The practical consequence of this result is that the copper precipitate contribution to RPV steel embrittlement saturates and is not expected to contribute to further increases in embrittlement during lifetime extension.

Positron Annihilation Spectroscopy Results

During the course of this LDRD research project, we have experimentally characterized more than 50 specimen composition and neutron irradiation conditions by positron annihilation spectroscopy. The alloys consisted of simple binary and ternary Fe-based alloys, model reactor pressure vessel steels and actual reactor pressure vessel weld steels by positron annihilation spectroscopy, which were neutron irradiated over a wide range of neutron flux, fluence and temperature, representative of the anticipated end of life exposures for current nuclear power plants. The specimens were provided by Professor G. Robert Odette of the University of California, Santa Barbara and returned to UCSB after the measurements were completed. Additionally, these PAS measurements were complemented by small angle neutron scattering characterization, performed in collaboration with UCSB. The results of these measurements have been disseminated in 7 journal and 6 conference proceedings publications (as listed in the bibliography) and been presented at international conferences. Selected results will be presented in this final report.

Orbital Electron Momentum Spectroscopy (OEMS) for binary Fe-0.9wt% Cu and ternary Fe-0.9 wt% Cu-1.0wt% Mn alloys following neutron irradiation are presented in Figure 2, with the irradiation conditions presented in Table 2. The data are normalized by the corresponding spectrum from the un-irradiated reference specimen in order to emphasize the high momentum portion of the spectra; i.e., $n(p_L)/n(p_L)_{reference}$. Thus, the un-irradiated reference specimen would have a horizontal line at 1 in this figure. Also included in the figure is a correspondingly referenced spectrum of well-annealed elemental copper. The spectra for the irradiated alloys clearly show evidence of copper, as seen by the peak at $p_L \sim 3.5$ atomic units (a.u.). The OEMS for the Fe-Cu alloy, shown in Fig. 2a, reveals an increasing peak in the low momentum spectrum ($p_L < 0.75$ a.u.) with increasing neutron fluence, while the broad peak at $p_L \cong 3.5$ a.u. decreases. The increase in the low momentum portion results from an increased fraction of positrons annihilating with valence electrons, and indicates positron localization and annihilation at vacancy clusters. The OEMS evolution with increasing fluence, that is an increase at $p_L < 0.75$ a.u. and a decrease $p_L \cong 3.5$ a.u., is consistent with a two-defect trapping model, where the dominant positron trap evolves between the copper rich precipitates (~3.5 a.u.) and a secondary feature (< ~0.75 a.u.), identified as vacancy solute clusters. This change in the low momentum fraction and its identification as trapping and annihilation at vacancy clusters is confirmed by the magnetic polarization along with positron lifetime measurements, plotted in Figures 3 and 4 and discussed below.

Table 2 - Neutron irradiation conditions, all irradiations were performed at T = 290°C.

Irradiation Designation	neutron flux [ϕ (n/m^2-s)]	neutron fluence [ϕt (n/m^2)]
A1	7. 0×10^{14}	6.0×10^{20}
A2	7.0×10^{14}	1.0×10^{21}
A3	7.0×10^{14}	2.3×10^{21}
A4	7.0×10^{14}	3.2×10^{21}
A5	5.0×10^{15}	4.0×10^{21}

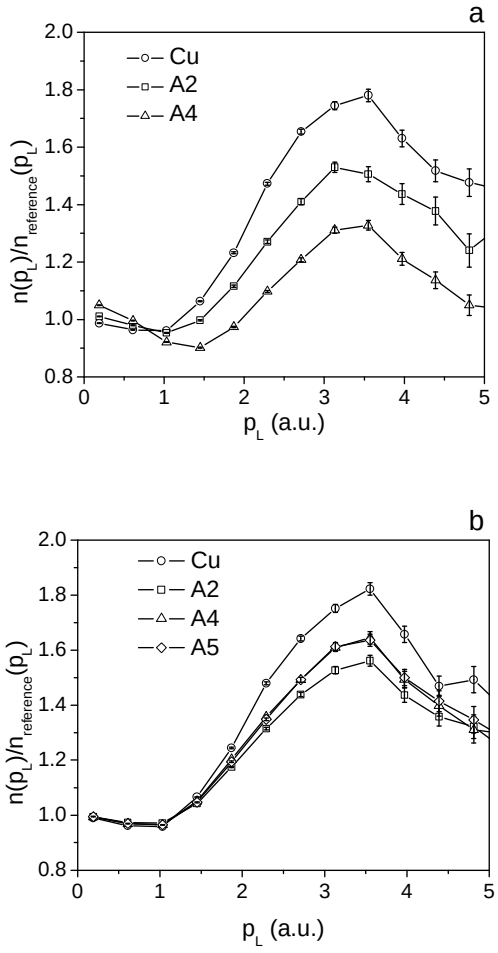

Figure 2 - Orbital electron momentum spectra for the a) Fe-Cu and b) Fe-Cu-Mn alloys irradiated under different conditions (Table 2). The spectra have been normalized to the corresponding un-irradiated reference specimen. The correspondingly normalized curves of elemental Cu are shown for comparison.

The measured OEMS for the Fe-Cu-Mn alloy, shown in Fig. 2b, does not vary with fluence and is quite similar to the shape of the copper spectrum, although with a slightly decreased magnitude. These spectra are indicative of copper precipitates that are highly enriched in Cu. Annihilations with either Fe or Mn would reduce the OEMS magnitude, and values for annihilations with Mn electrons are less than 1.0, relative to Fe, at high electron momentum (p_L > 2 a.u.). Thus, a CRP composition of 89.5% Cu, 10.5% Mn obtained from the measured M/N ratio by SANS is consistent with the measured OEMS spectrum. Another interesting note is the lack of a peak in the OEMS spectra at low momentum values (and a corresponding lack of long lifetime components, discussed below) in the Fe-Cu-Mn alloy. This may suggest that Mn retards the formation of large vacancy-solute clusters; or, alternately, the effect of Mn on the CRP population increases the number density to a level where all of the positrons localize in the CRPs.

The results of the spin-polarized, magnetic positron annihilation measurements are presented in Figure 3. For both the Fe-Cu and the Fe-Cu-Mn alloys, the un-irradiated reference specimen has a split in the two points with the magnetic field oriented parallel and anti-parallel to the positron spin, similar to the iron sample. For all the irradiated specimens, the two points nearly super-impose with a significant reduction in the splitting, similar to the copper sample. This lack of splitting with magnetic field reversal is an indication of non-magnetic behavior at the region of positron annihilation. Figure 3 also shows that the fraction of annihilations with low momentum electrons increases with increasing fluence for the Fe-Cu alloy, again a characteristic of increasing annihilations with valence electrons and indicative of trapping in vacancy clusters.

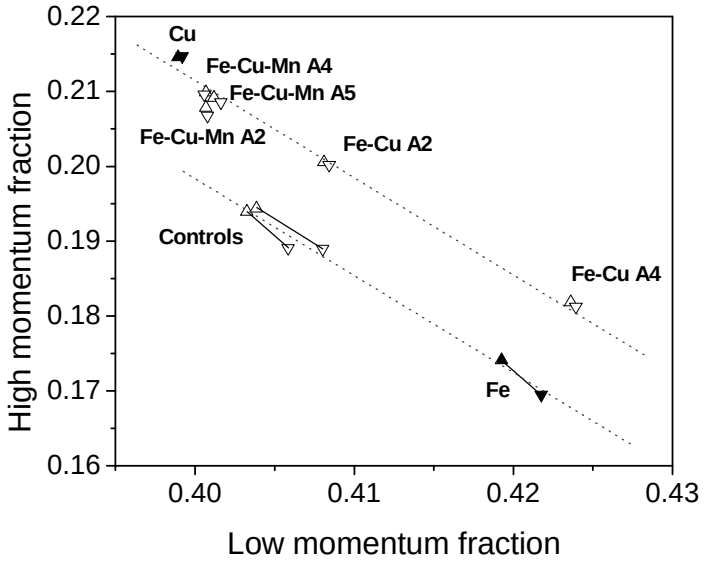

Figure 3 - Results of the spin-polarized, magnetic positron annihilation measurements. Positron annihilation fraction with high momentum (1-4 a.u.) versus low momentum (< 0.38 a.u.) electrons, normalized to the total annihilations, for the magnetic field oriented parallel (up triangle) and anti-parallel (down triangle) to the positron polarization. Elemental Fe and Cu are shown with solid symbols. The dotted lines are drawn to guide the eye.

Positron annihilations with high momentum electrons (orbital electrons) give a measure of the chemical composition of the region in which the positron annihilates. Positron annihilation with low momentum electrons (valence electrons) give a measure of the vacancy character of the region in which the position annihilates. When OEMS data are plotted as in Figure 3, positron annihilations at a single type of defect at varying concentrations will lie along a single line. As shown by the dotted lines in Figure 3, drawn to guide the eye, the un-irradiated control specimens are consistent with a single line with elemental Fe, while the irradiated samples are consistent with a different single line with elemental Cu. This simple analysis also strongly indicates the highly enriched nature of Cu in the precipitates.

Positron lifetime annihilation spectroscopy data is presented in Figure 4. For the Fe-Cu alloy, Fig. 4a, the mean positron lifetime increases with increasing neutron fluence. The positron lifetime fitting procedure yielded two distinct lifetime components at a fluence of 1.0×10^{21} n/m^2, with the second lifetime component of 222 ps consistent with small vacancy clusters. The fitting procedure yielded three lifetime components for the specimens irradiated to higher fluence, with the two longer lifetime components (of approximately 210 and 375 ps) consistent with small and larger vacancy clusters, respectively. As already mentioned, the OEMS results of Fig. 2 and 3 provide an indication that the vacancy clusters are likely complexed with Cu solutes.

The mean lifetime in all of the Fe-Cu-Mn irradiated alloys, shown in Fig. 4b, was 116 ps, compared to 109 ps for the reference alloy. The positron lifetime fitting procedure yielded only one lifetime component in all of the Fe-Cu-Mn alloys. The increase in mean lifetime is consistent with positron lifetime calculations using a recently developed electronic structure method [13] of 107 ps for bulk Fe and 111 ps for Cu in a BCC structure with the Fe lattice constant and likely indicate positron confinement in CRPs. Notably, no longer lifetime components are observed in PALS for the irradiated Fe-Cu-Mn alloys, consistent with the lack of low momentum peak of the OEMS (Figure 2).

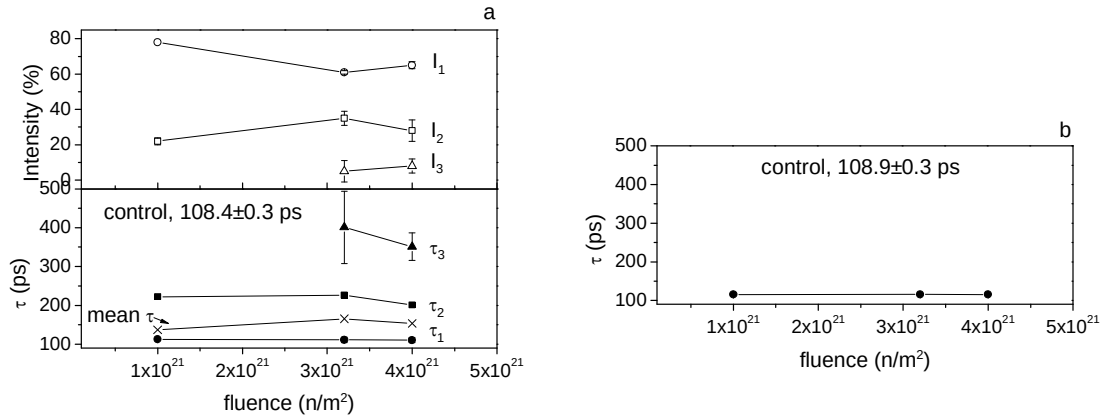

Figure 4 - Results of the PALS for the a) Fe-Cu and b) Fe-Cu-Mn alloy. Lifetimes for the reference specimens are indicated on the graphs. For the Fe-Cu alloy, the bottom panel shows lifetime, including mean lifetime, while the upper panel shows the intensity of each lifetime component. Three lifetimes were present in the Fe-Cu alloy at the higher fluence levels, while the Fe-Cu-Mn alloy only exhibited a single lifetime.

The results of measurements on model reactor pressure vessel steels and actual reactor pressure vessel welds are remarkably similar to the results on binary and ternary alloys, showing that the positrons are also sensitive probes of the nanometer-sized copper precipitates even in steels with high dislocation densities and complex microstructures. Figure 5 shows the measured magnetic polarization OEMS results for a model reactor pressure vessel steels (LC, which contains 0.4% Cu, 0.8% Ni and 1.4% Mn) and two actual reactor pressure vessel welds (WG and WV, both of which contain >0.25% Cu, ~1.5% Ni and 1.2% Mn). These OEMS results for the reactor pressure vessel steels and welds all lie on a single line, away from Fe, similar to the results of Figure 3, and indicate that the precipitates are non-magnetic. It is important to note that some magnetic splitting is observed for LC T11 and T12 and the WV and WG alloys. However, SANS results on these specimens indicated that the precipitates were extremely small and were more enriched in Ni. Thus, it is likely that the relatively small magnetic splitting observed results from either the contribution of positron annihilations with nickel electrons (note the splitting for elemental Ni) or partial positron confinement in the precipitates due to their smaller size.

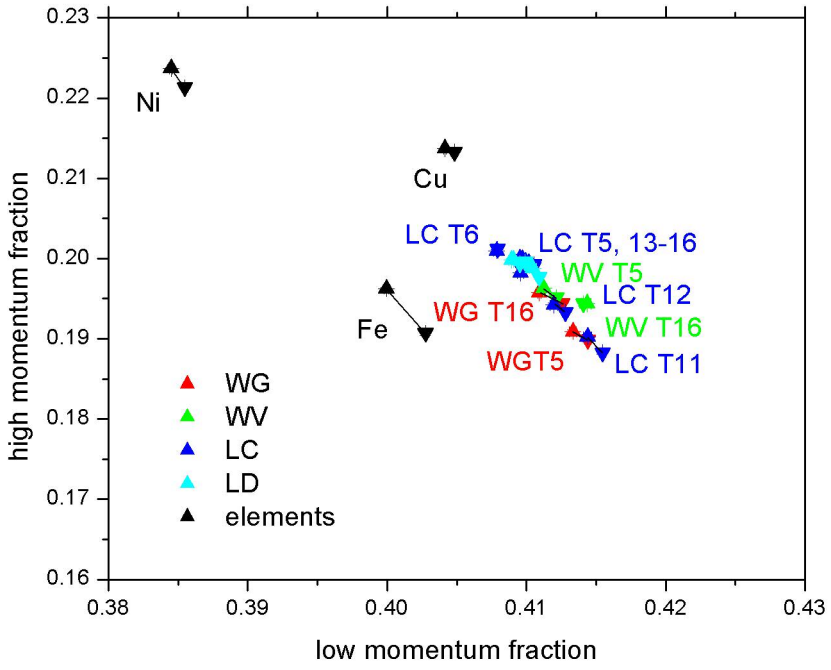

Figure 5 - Results of spin-polarized, magnetic positron annihilation measurements of reactor pressure vessel model steels (designated LC and LD) and welds (designated WG and WV). Positron annihilation fraction with high momentum (1-4 a.u.) versus low momentum (< 0.38 a.u.) electrons is plotted, normalized to the total annihilations, for the magnetic field oriented parallel (up triangle) and anti-parallel (down triangle) to the positron polarization. The designation T5, T11-16 denotes the irradiation conditions at approximately 290°C.

Comparison of modeling and experimental results

The prediction of sub-nanometer nanovoids and vacancy-copper clusters in Fe-Cu alloys (shown in Figure 1) has been experimentally validated within this program using positron

annihilation spectroscopy (shown in Figure 2), aided by direct comparison between the measured positron observables. Figure 6a shows the atomic configuration of one vacancy – copper cluster predicted by the cascade aging simulations, in this case containing 17 vacancies and 5 Cu atoms. This atomic configuration was the input for a quantum mechanical simulation to calculate the positron probability density (wave function) shown in Figure 6b and subsequently, to predict the orbital electron momentum spectrum (OEMS) measured in PAS experiments. Figure 6c shows the predicted OEMS for elemental Cu, a 17 vacancy-5 Cu atom cluster and a 4 vacancy-6 Cu atom cluster. Figure 6d shows the corresponding measured OEMS spectrum in a Fe-0.9% Cu alloy neutron irradiated to $0.3x10^{23}$ n/m^2 at 60°C. The OEMS spectra shown in Figures 6c and 6d plot the number of positron annihilations at a given electron momentum, normalized to pure, unirradiated Fe. Both the simulated and measured OEMS clearly show a peak in the number of annihilations at low momentum values, which is characteristic of vacancy clusters, and a second, broader peak at higher momentum, which is characteristic of Cu. Further, the predicted lifetime from quantum mechanical simulations for the vacancy-copper cluster shown in Figure 6a was 350 ps, which agrees well with the positron lifetime component of 355 ps experimentally measured with a relative intensity of nearly 30%. The qualitative agreement between the predicted and measured OEMS and quantitative agreement in positron lifetimes provides experimental validation of our prediction of the features formed in this alloy under irradiation.

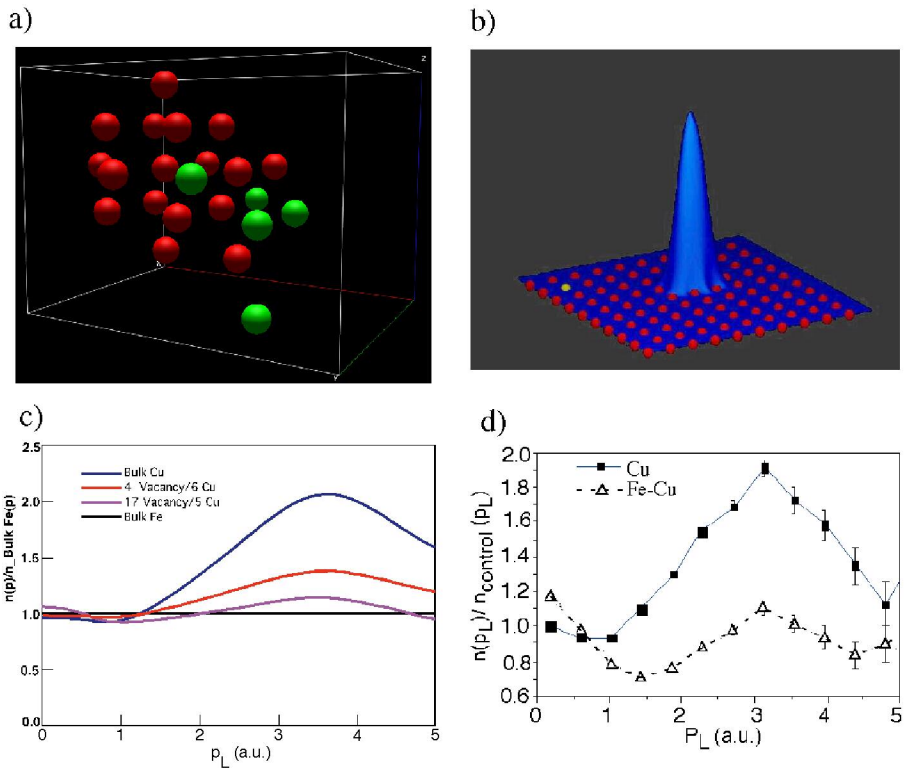

Figure 8. a) Atomic configuration of a three dimensional, sub-nanometer, 17 vacancy (red)-5 copper (green) cluster formed during cascade aging; b) positron wave function localized within the cluster, as simulated by a quantum mechanical code [13]; c) the predicted Orbital Electron Momentum Spectra (OEMS) for elemental Fe (black), elemental Cu (blue), a 4 vacancy-6 copper cluster (red) and the 17 vacancy-5 copper cluster (purple) of Figure 9a, normalized to elemental Fe; d) the measured OEMS, normalized to the unirradiated Fe-0.9%Cu control, for elemental copper (black squares) and the Fe-0.9% Cu alloy irradiated at 60°C (open triangles).

SUMMARY

The technical outcome of this LDRD project is resolution of the two outstanding questions regarding reactor pressure vessel embrittlement. Namely, we have shown through a combination of modeling and novel positron annihilation spectroscopy experiments that the nanometer-sized copper precipitates do not contain significant quantities of Fe. As well, we have positively identified the secondary embrittling feature, or so-called matrix features, as sub-nanometer vacancy – copper solute cluster complexes. The results clearly show that the precipitates are non-magnetic and place an upper limit of ~10% for the Fe content of the precipitates. This is in agreement with SANS, but at odds with recent 3DAP measurements. The practical consequence of this result is that the copper precipitate contribution to RPV steel embrittlement saturates and is not expected to contribute to further increases in embrittlement during lifetime extension. Finally, our study demonstrates that polarized positrons can be used as a powerful probe of the magnetic character of nanoscale materials, even when they are embedded in a magnetic matrix.

REFERENCES

1. G.R. Odette, B.D. Wirth, D.J. Bacon, and N.M. Ghoniem, "Multiscale-Multiphysics Modeling of Radiation-Damaged Materials: Embrittlement of Pressure-Vessel Steels", MRS Bulletin, March 2001, p. 176.
2. G. R. Odette, *MRS Soc. Symp. Proc.* 373 (1995) 137.
3. P. Pareige and M. K. Miller, *App. Surf. Sci.* 94/95 (1996) 370.
4. E. D. Eason, J. E. Wright, and G. R. Odette, Improved Embrittlement Correlations for Reactor Pressure Vessel Steels, NUREG/CR-6551, (1998).
5. M.J. Caturla, N. Soneda, E.A. Alonso, B.D. Wirth and T. Diaz de la Rubia, *J. Nuc. Mat.*, **276** (2000) p. 13.
6. M.W. Finnis and J.E. Sinclair, *Phil. Mag.* **A 50 (1)** (1984) 45.
7. G. J. Ackland, G. I. Tichy, V. Vitek, and M. W. Finnis, *Phil. Mag.* **A 56** (1987) 735.
8. B.D. Wirth and G.R. Odette, *MRS Soc. Symp. Proc.* **481** (1998) 151.
9. P. Hautojärvi and C. Corbel, Positron Spectroscopy of Solids, Proceedings of the International School of Physics, Course CXXV, edited by A. Dupasquier and A.P. Mills, Jr. (Bologna, Italy: Italian Physical Society), (1995) 491 – 532.
10. P. Asoka-Kumar, M. Alatalo, V.J. Ghosh, A.C. Kruseman, B. Nielsen, and K.G. Lynn, *Phys Rev Let* **77** (1996) 2097.
11. M.J. Puska and R.M. Nieminen, *Rev. Mod. Phys.* **66** (1994) 841.
12. Y. Nagai, M Hasegawa, Z. Tang, A. Hempel, K. Yubata, T. Shimamura, Y. Kawazoe, A. Kawai and F. Kano, *Phys. Rev. B* **61** (2000) 6574.
13. P. A. Sterne, J. E. Pask and B. M. Klein, *App. Surf. Sci.* **149** (1999) 362.
14. S.S. Hanna and R.S. Preston, *Phys. Rev.* **109** (1958) 716-720.
15. S. Berko and J. Zukerman, *Phys. Rev. Lett.* **13** (1964) 339-341.
16. P. Genoud, A.K. Sing, A.A. Manuel, T. Jarlborg, E. Walker, M. Peter, and M. Weller, *J. Phys. F: Met. Phys.* **18** (1988) 1933-1947.
17. R.H. Howell, P.A. Sterne, J. Hartley, T.E. Cowan, *J. Appl. Surf. Sci.* **149** (1999) 103.

18. P. Asoka-Kumar, B.D. Wirth, P.A. Sterne, R.H. Howell, and G.R. Odette, *Philosophical Magazine Letters* **82** (2002) 609.
19. C.J. Glinka, J.M. Rowe and J.G. laRock, *J. of Applied Crystallography* **19** (1986) 427.
20. B.D. Wirth, PhD Thesis (1998), University of California, Santa Barbara.
21. B.D. Wirth, P. Asoka-Kumar, R.H. Howell, G.R. Odette, and P.A. Sterne, *MRS Soc. Symp. Proc* **650** (2001) R6.5.
22. M.K. Miller, B.D. Wirth and G.R. Odette, *Materials Science & Engineering A* **353** (2003) 133.
23**.** R.E. Stoller, *MRS Soc. Symp. Proc.* **373** (1995) 21.
24. A.F. Calder and D.J. Bacon, *J. Nucl. Mat.* **207** (1993) 25.
25. G.R. Odette and G.E. Lucas, *Radiation Effects & Defects in Solids* **144** (1998) p. 189.

BIBLIOGRAPHY

Refereed journal articles:

7. S.C. Glade, B.D. Wirth, P. Asoka-Kumar, G.R. Odette, P.A. Sterne, and R.H. Howell, "Positron Annihilation Spectroscopy and Small Angle Neutron Scattering Characterizations of the Effect of Mn on the Nanostructural Features formed in Irradiated Fe-Cu-Mn Alloys", accepted for publication, *Phil. Mag., UCRL-JC-152567.*

6. S.C. Glade, B.D. Wirth, P. Asoka-Kumar, P.A. Sterne, and G.R. Odette, "Positron Annihilation Spectroscopy of Nanostructural Features in Model Reactor Pressure Vessel Steels", *Materials Science Forum*, **445-446** (2004) 87, UCRL-JC-154520.

5. M.K. Miller, B.D. Wirth and G.R. Odette, "Precipitation in Neutron Irradiated Fe-Cu and Fe-Cu-Mn Model Alloys: A Comparison of APT and SANS Data", *Materials Science & Engineering A* **353** (2003) 133.

4. P. Asoka-Kumar, B.D. Wirth, P.A. Sterne, R.H. Howell, and G.R. Odette, "Composition and magnetic character of nanometer-size Cu precipitates in reactor pressure vessel steels: implications for nuclear power plant lifetime extension", *Philosophical Magazine Letters* **82** (2002) 609.

3. P. Asoka-Kumar, R. Howell, T.G. Nieh, P.A. Sterne, B.D. Wirth, R.H. Dauskardt, K.M. Flores, D. Suh, G.R. Odette, "Opportunities for materials characterization using high-energy positron beams", *Applied Surface Science* **194** (2002) 160.

2. S. Jumel, C. Domain, J. Ruste, J.-C. Van Duysen, C. Becquart, A. Legris, P. Pareige, A. Barbu, E. Van Walle, R. Chaouadi, M. Hou, G.R. Odette, R.E. Stoller, and B.D. Wirth, "Simulation of Irradiation Effects in Reactor Pressure Vessel Steels: the Reactor for Virtual Experiments (REVE) Project", *Journal of Testing and Evaluation*, **30** (2002) 37.

1. G. R. Odette, B. D. Wirth, D. J. Bacon and N. M. Ghoneim, “Multiscale-Multiphysics Modeling of Radiation-Damaged Materials: Embrittlement of Pressure Vessel Steels”, MRS Bulletin, **26** (2001) 176.

Conference proceedings

6. S.C. Glade, P. Asoka-Kumar, T.G. Nieh, P.A. Sterne, B.D. Wirth, R.H. Dauskardt, K.M. Flores, D. Suh, and G.R. Odette, “Bulk materials analysis using high-energy positron beams”, accepted for publication, Amer. Inst. Of Physics Conf. Proceedings (2004), UCRL-JC-151599.

5. R.E. Stoller, M.K. Miller, G.R. Odette, and B.D. Wirth, “Contributions of fundamental studies to understanding RPV embrittlement”, *Transactions of the American Nuclear Society*, **88** (2003) 539.

4. B.D. Wirth and G.R. Odette, “Recent progress towards a mechanistic model of reactor pressure vessel embrittlement”, Proceedings of the International Symposium on the Mechanisms of Material Degradation and Non-Destructive Evaluation in Light Water Reactors, Institute of Nuclear Systems Safety, Osaka, Japan (2002) 77.

3. B.D. Wirth, G.R. Odette, P. Asoka-Kumar, R.H. Howell, and P.A. Sterne, “Characterization of Nanostructural Features in Irradiated Reactor Pressure Vessel Model Alloys”, Proceedings of the 10th International Symposium on Environmental Degradation of Materials in Light Water Reactors, Ed., G.S. Was, National Association of Corrosion Engineers, 2002.

2. B.D. Wirth, G.R. Odette and R.E. Stoller, “Recent Progress Toward an Integrated Multiscale-Multiphysics Model of Reactor Pressure Vessel Embrittlement”, *MRS Soc. Symp. Proc* **677** (2001) AA5.2.

1. B.D. Wirth, P. Asoka-Kumar, R.H. Howell, G.R. Odette, and P.A. Sterne, “Positron Annihilation Spectroscopy and Small Angle Neutron Scattering Characterization of Nanostructural Features in Irradiated Fe-Cu-Mn Alloys”, *MRS Soc. Symp. Proc* **650** (2001) R6.5